Polo-like kinase 1 regulates immune synapse assembly and cytotoxic T cell function by driving microtubule dynamics

Polo-like kinase 1 regulates immune synapse assembly and cytotoxic T cell function by driving microtubule dynamics

Fabrizia Zevolini[1], Anna Onnis[1], Roxana Khazen[2], Sabina Müller[2], Giuseppe Marotta[3], Salvatore Valitutti[2], Francesca Finetti[1#] and Cosima T Baldari[1#]

[1]Department of Life Sciences, University of Siena, Siena, Italy; [2] INSERM U1037, Centre de Recherche en Cancérologie de Toulouse (CRCT), Toulouse, France; [3]Siena University Hospital, Siena, Italy.

[#]shared senior authorship

Corresponding authors: Dr. Francesca Finetti, Department of Life Sciences, University of Siena, Via Aldo Moro 2, 53100 Siena, Italy, tel +39-0577-232427, email finetti4@unisi.it; Dr. Cosima T Baldari, Department of Life Sciences, University of Siena, Via Aldo Moro 2, 53100 Siena, Italy, tel +39-0577-234400, email cosima.baldari@unisi.it

Running title: PLK1 regulates CTL polarization

Keywords: immune synapse / cytotoxic T cell / centrosome / microtubules / PLK1

Summary statement

The mitotic kinase Polo-like kinase 1 promotes centrosome polarization to the immune synapse in cytotoxic T cells by coupling TCR signaling to microtubule dynamics

Abstract

Elimination of virally infected or tumoral cells is mediated by cytotoxic T cells (CTL). Upon antigen recognition CTLs assemble a specialized signaling and secretory domain at the interface with their target, the immune synapse (IS). During IS formation CTLs acquire a transient polarity, marked by re-orientation of the centrosome and microtubule cytoskeleton toward the IS, thus directing the transport and delivery of the lytic granules to the target cell. Based on the implication of the kinase Aurora-A in CTL function we hypothesized that its substrate, the mitotic regulator Polo-like kinase 1 (PLK1), may participate in CTL IS assembly. We demonstrate that PLK1 is phosphorylated upon TCR triggering and polarizes to the IS. PLK1 silencing or inhibition results in impaired IS assembly and function, as witnessed by defective synaptic accumulation of TCRs as well as compromised centrosome and lytic granule polarization to the IS, resulting in impaired target cell killing. This function is achieved by coupling early signaling to microtubule dynamics, a function pivotal for CTL-mediated cytotoxicity. These results identify PLK1 as a new player in CTL IS assembly and function.

Introduction

Cytotoxic T cells (CTL) are the arm of adaptive immunity specialized in the elimination of virally infected or tumoral cells. To achieve this function CTLs have evolved three complementary mechanisms that function sequentially to allow for the serial killing of cognate targets. The first involves the lytic granules (LG), which are specialized secretory lysosomes enriched in the pore-forming toxin perforin (Prf) and the proteolytic enzymes granzymes (Gzm) packed on a serglycin scaffold to form a dense core that is solubilized upon LG exocytosis. Gzms are then delivered to cell targets through pores formed by Prf polymerization to orchestrate their apoptotic demise (Cassioli and Baldari, 2022; McKenzie and Valitutti, 2023). The second, which is essential for the sustained killing activity of CTLs when their LG stores become exhausted, is mediated by the death receptor ligand FasL, that triggers the apoptotic cascade initiated by caspase 8 through interaction with Fas on target cells (Green and Llambi, 2015; Cassioli and Baldari, 2022). A third mechanism that has been recently discovered involves the release of supramolecular attack particles (SMAP), autonomous killing entities that are composed of a core contaning Prf and Gzms enclosed in a non-membranous glycoprotein shell (Balint et al., 2020) and stored in a different type of LG, the multicore cytotoxic granule (Chang et al., 2022; Cassioli and Baldari, 2022).

CTL-mediated killing requires the assembly of the immune synapse (IS), a specialized signaling and secretory platform that forms at the cell target interface (De La Roche et al., 2016). TCR interaction with MHC-bound cognate peptide antigen on the target cell surface triggers a signaling cascade that promotes the translocation of the centrosome and associated microtubule cytoskeleton beneath the synaptic membrane, resulting in the acquisition by the CTL of a transient polarity (Gomez and Billadeau, 2008; Huse et al., 2013). This polarity is essential for the directional transport of the LGs and FasL-enriched vesicles towards the target cell and their precise delivery at the IS, thus ensuring the selective killing of the cognate target.

A tight interplay of the tubulin and actin cytoskeletons coordinates the movement of the centrosome towards the IS, with microtubule (+) ends interacting with F-actin at the IS periphery with the assistance the adaptors IQ-GAP, ezrin and Cdc42IP (Banerjee et al., 2007; Gorman et al., 2012; Ilani et al., 2007). Regulators of microtubule and actin dynamics,

including the dynein/dynactin motor, the microtubule end-binding protein EB1, the small GTPase Rac1, the formins mDia and INF2, and the histone deacetylase HDAC6 also contribute to this process (Andrés-Delgado et al., 2013; Bouchet et al., 2016; Gomez and Billadeau, 2008; Martín-Cófreces et al., 2012; Sanchez et al., 2019; Serrador et al., 2004). Centrosome positioning at the IS center is paralleled by F-actin clearance to leave an actin-poor region that facilitates LG exocytosis (Ritter et al., 2015). The signals that regulate centrosome polarization in response to TCR triggering are as yet only partly defined. PLCγ activation downstream of early TCR signaling has been identified as a key initiating event. Diacyl glycerol produced by PLCγ at the IS center acts as a polarity determinant to attract the atypical PKCs such as ζ (Huse et al., 2013). These kinases orchestrate the process of centrosome translocation through phosphorylation of regulators of cytoskeleton dynamics such as myosin II, that interacts with the dynein/dynactin complex to provide the pulling forces required for centrosome movement (Liu et al., 2013).

Interestingly, the mitotic serine-threonine kinase Aurora A (AurA) has been recently implicated in the signaling events leading to IS formation in $CD4^+$ T cells (Blas-Rus et al., 2016). In mitotic cells AurA expression and activity peak in late G2, when the protein is concentrated at centrosomes (Bischoff, 1998). During mitosis AurA regulates centrosome and spindle dynamics by recruiting microtubule nucleation and stabilization factors (Sardon et al., 2008). In non-dividing $CD4^+$ T cells AurA is activated upon TCR stimulation and modulates TCR signaling to regulate the growth of the microtubules arising from the centrosome, thereby facilitating the polarized vesicular traffic that is essential for T cell activation and effector function (Blas-Rus et al., 2016). Here we have investigated the role of the mitotic kinase PLK1, a key substrate of AurA controlling centrosome and microtubule dynamics during cell cycle progression (Joukov and De Nicolo, 2018), in CTL IS assembly. We show that PLK1 is associated with the centrosome and is co-mobilized to the IS, where a pool of active PLK1 associates with the synaptic membrane. We provide evidence that PLK1 subserves AurA-dependent and -independent functions in CTLs, where it promotes centrosome polarization to the IS and the downstream events leading to target cell killing by coupling TCR signaling to microtubule growth. Our results identify PLK1 as a new player in CTL IS assembly and effector function.

Results

PLK1 is recruited to the CTL IS together with the centrosome and is activated in response to TCR signaling

PLK1 has been reported to localize at the centrosome in a variety of cell types (Colicino and Hehnly, 2018), hyet its localization in T lymphocytes is presentòy elusive. To address this point we generated CTLs from peripheral blood $CD8^+$ T cells freshly purified from healthy donors and activated using beads coated with anti-CD3 and anti-CD28 mAbs in the presence of IL-2. Under these conditions $CD8^+$ T cells differentiate to fully functional CTLs by day 5-7 (Onnis et al., 2023).

Immunoblot analysis showed that PLK1 is expressed in freshly purified $CD8^+$ T cells and that its expression is increased during their differentiation to CTLs (Fig.1A). To determine the intracellular localization of PLK1 in CTLs we carried out a confocal microscopy analysis of CTLs co-stained for PLK1 and either pericentriolar material 1 (PCM1), a centriolar satellite protein that is responsible for PLK1 recruitment to the pericentriolar matrix (Wang et al., 2013), or the centrosome marker γ-tubulin. Similar to other cell types, PLK1 was found to localize at the centrosome in CTLs (Fig.1B). PLK1 also co-localized with the centrosome in CMV-specific T cell clones (Fig.S1A,B) and in other T cell settings, including Jurkat T cells and freshly purified peripheral blood $CD4^+$ T cells (Fig.S2A). AurA also displayed a centrosomal localization in CTLs (Fig.S3A,B), as previously reported for $CD4^+$ T cells (Blas-Rus et al., 2016).

To assess whether PLK1 could participate in centrosome dynamics during IS formation, we carried out a similar co-localization analysis in conjugates of CTLs with Raji B cells pulsed with a mix of staphylococcal superantigens (SAgs) allowing for the polyclonal activation of T cells independently of antigen specificity. The analysis was carried out either 5 or 15 minutes after conjugate formation to visualize the events taking place during IS assembly (De La Roche et al., 2016). PLK1, as well as AurA, were found to localize at the CTL subsynaptic region in association with the centrosome as early as 5 min after conjugate formation (Fig.1C; Fig.S3A,C). Similar results were obtained in antigen-specific conjugates formed using CMV-specific $CD8^+$ T cell clones (Fig.S1A,C). PLK1 co-polarized with the

centrosome to the IS also in Jurkat T cells and freshly purified peripheral blood $CD4^+$ T cells (Fig.S2B,C).

The kinase activity of PLK1 depends on its phosphorylation by AurA and its co-factor Bora on the T-loop Thr210 residue (Bruinsma et al., 2013). Immunoblot analysis of the phosphorylated, active form of PLK1 (pPLK1) revealed that, while pPLK1 was barely detectable in unstimulated cells, there was a sharp increase in response to TCR engagement, with the highest levels detected at the earliest time point analyzed (Fig.1D). To assess the specific localization of activated PLK1 at the IS, we performed a confocal microscopy analysis of pPLK1 in CTLs conjugated with either SAg-pulsed or unpulsed Raji B cells. pPLK1 could be detected at the centrosome in conjugates formed both in the absence of and in the presence of SAgs (Fig.1E). Additionally, pPLK1 was detectable at the IS in SAg-specific conjugates (Fig.1E). Hence PLK1 polarizes to the IS in association with the centrosome and a pool of its active form accumulates at the synaptic membrane, suggesting a potential implication in CTL IS formation.

PLK1 is required for IS formation and TCR signaling in CTLs

IS formation is marked by the accumulation of TCR complexes at the central area of the T cell interface with the APC. Two TCR pools, of which one associated with the plasma membrane and the other with recycling endosomes, are sequentially recruited to the IS following TCR engagement by cognate antigen, thereby ensuring sustained TCR signaling (Soares et al., 2013). To investigate the potential role of PLK1 at the CTL IS we took advantage of the highly selective ATP analogue BI2536, which inhibits PLK1 activity at low nanomolar concentrations (Steegmaier et al., 2007). Confocal microscopy analysis of SAg-specific CTL conjugates revealed that the synaptic accumulation of TCRs was impaired in BI2536-treated CTLs, as assessed by labelling the CD3ζ chain of the TCR complex (Fig.2A), indicating that PLK1 is required for IS formation in CTLs. Similar results were obtained on Jurkat and freshly purified peripheral $CD4^+$ T cells (Fig.S2D,E). To rule out off-target effects of BI2536, TCR accumulation at the IS was also analyzed on SAg-specific conjugates formed with CTLs where PLK1 expression was silenced by RNA interference (Fig.2B). PLK1 KD CTLs recapitulated the defect observed in BI2536-treated CTLs (Fig.2C), supporting the key role of PLK1 in IS formation. PLK1 blockade resulted in defective synaptic TCR

accumulation also in Jurkat T cells and freshly purified peripheral blood $CD4^+$ T cells (Fig.S2D,E).

The PLK1 upstream activator AurA has been implicated in early TCR signaling by promoting the activatory phosphorylation and synaptic localization of the initiating kinase Lck in $CD4^+$ T cells (Blas-Rus et al., 2016). To understand whether PLK1 may mediate this effect of AurA in CTLs we imaged the active form of Lck, phosphorylated on Y394, in BI2536- treated CTLs conjugated with SAg-pulsed Raji cells. A defect in the IS accumulation of active Lck was observed in PLK1-inhibited CTLs (Fig.3A). Inhibition of Lck phosphorylation on Y394 in the presence of BI2536 was also observed by immunoblot analysis of post-nuclear supernatants from CTLs activated by antibody-mediated TCR cross-linking (Fig.3B). Consistent with this defect, immunoblot analysis of the active forms of two proteins that participate at sequential steps in the signaling cascade downstream of Lck, namely the transmembrane adaptor LAT and the kinase Erk1/2 (Samelson, 2002), showed that BI2536 treatment led to an impairment in TCR-dependent LAT and Erk phosphorylation (Fig.3C). The results indicate that PLK1 regulates the TCR signaling cascade in CTLs, accounting for its requirement for IS formation.

PLK1 is required for centrosome and LG polarization to the IS and for CTL-mediated killing

Centrosome translocation toward the T cell interface with cognate APC occurs in response to TCR engagement and in turn orchestrates the polarized recycling of endosome-associated TCRs to the synaptic membrane (Das et al., 2004). In CTLs, centrosome reorientation toward the IS, concomitant with the dynamic reorganization of the microtubule cytoskeleton, ensures the polarized transport of LGs along the microtubules to the site of contact and the release of their contents into the synaptic cleft (Douanne and Griffiths, 2021; Kabanova et al., 2018). Confocal analysis of SAg-specific conjugates formed with BI2536-treated CTLs showed an impairment in both centrosome and LG repositioning beneath the IS membrane, as assessed by quantifying both the frequency of conjugates harboring centrosome and LG polarization at the IS and their distance from the synaptic membrane (Fig.4A,B,C). Similar results were obtained using PLK1 KD CTLs (Fig.4E,F) and a CMV-specific CTL clone (Fig.S1D,E,F). Furthermore, LG convergence around the centrosome,

which occurs in preparation for their transport to the IS (Calvo and Izquierdo, 2021), was impaired in BI2536-treated CTLs, as assessed by measuring the distance of individual GzmB$^+$ vesicles from the PCNT-1 positive compartment (Fig.4D). This defect was recapitulated in PLK1 KD CTLs (Fig.4G). The inhibitory effect of BI2536 on centrosome polarization was also observed in CMV-specific CTL clone (Fig.S1G), Jurkat and freshly purified peripheral CD4$^+$ T cells (Fig.S2D,E).

PLK1 promotes microtubule growth in CTLs

Upon TCR stimulation, microtubule filaments and microtubule motor proteins anchored at the cell cortex at the CTL interface with its cell target provide the pulling forces for centrosome translocation (Kuhn and Poenie, 2002). Microtubules are large polymers composed of α/β-tubulin dimers that are endowed with an intrinsic polarity, with (-) ends anchored to the centrosome to avoid rapid depolymerization and (+) ends characterized by dynamic instability (Li and Gundersen, 2008). After centrosome polarization, microtubules actively polymerize at the IS. Altering microtubule (+) end dynamics delays centrosome reorientation and vesicular traffic to the IS (Hooikaas et al., 2020; Martín-Cófreces et al., 2012), underscoring the importance of microtubule plasticity in the establishment of a functional IS.

PLK1 plays a crucial role in orchestrating microtubule dynamics in cycling cells (Zitouni et al., 2014). We hypothesized that the architecture of the microtubule cytoskeleton might be altered in PLK1-inhibited CTLs. To address this point, we imaged control and BI2536-treated CTLs plated under non-activating conditions (poly-L-lysine) and stained for α-tubulin. Control CTLs displayed numerous thin microtubules radiating from the centrosome (Fig.5A,B). When PLK1 activity was inhibited, microtubules organized in thick bundles that in some cases appeared to originate in the cortical area (Fig.5A,B). To quantify this feature we measured the skewness of pixel intensity, an amply validated method for the quantitative detection of bundling of actin filaments and microtubules (Higaki, 2010; Higaki, 2017). The skewness of the fluorescence intensity distribution becomes higher when the number of pixels with high fluorescence intensity is increased, providing a quantitative and reliable measurement of cytoskeleton bundling. BI2536-treated CTLs showed a higher skewness in

α-tubulin staining compared to control cells (Fig.5C), providing evidence that PLK1 is involved in the regulation of the architecture of the microtubule cytoskeleton in CTLs.

Since microtubule dynamics regulates the polarization of the centrosome to the IS (Stinchcombe and Griffiths, 2014), we asked whether the TCR signaling defect observed in BI2536-treated CTLs under steady-state conditions may impact on microtubule growth during IS assembly. CTLs were transiently transfected with a plasmid construct encoding EGFP-tagged EB1, a protein that binds to the (+) end of growing microtubules (Nehlig et al., 2017), and plated on glass-immobilized anti-CD3 mAb to induce centrosome polarization and microtubule polymerization (Bunnell et al., 2002). The dynamics of microtubule growth following CTL stimulation was tracked by EB1-EGFP live cell imaging and total internal reflection fluorescence (TIRF) microscopy to improve spatial and time resolution (Dixit and Ross, 2010) (Fig.5D). BI2536-treated EB1-EGFP transfected CTLs displayed altered microtubule dynamics (Fig.5D-F; Movies 1,2). In particular, the number and length of each segment, identified as the portion of each EB1-EGFP labelled track with a constant trajectory, were decreased in CTLs following BI2536 treatment, showing that the directionality of newly formed tracks was affected when PLK1 was inhibited (Fig.5D-F). Furthermore, the growth of microtubules was slower in BI2536-treated CTLs compared to control cells (Fig.5D-F). Taken together, these results indicate that PLK1 regulates microtubule dynamics during IS assembly in CTLs.

PLK1 is required for efficient CTL-mediated killing

Rapid LG secretion upon target cell encounter can occur in the absence of centrosome translocation towards the IS membrane (Bertrand et al., 2013). Yet, the IS polarization of the CTL lytic machinery ensures the prolonged and confined secretion of lytic molecules onto the target cell, as demonstrated by the reduction in cytotoxicity when centrosome reorientation is delayed or defective (De La Roche et al., 2013; Jenkins et al., 2014; Tsun et al., 2011). To test the outcome of the IS defects associated with PLK1 inhibition on the killing capability of CTLs we performed a time course analysis of fluorescent calcein release by SAg-pulsed target cells induced by either BI2536-treated or untreated CTLs. In this assay target cells are loaded with the cell-permeant dye calcein AM, that becomes fluorescent following hydrolyzation by intracellular esterases and is released upon cell death (Chang et

al., 2018). Consistent with the role of PLK1 in TCR signaling and IS assembly, the killing capability of CTLs was impaired at every effector:target cell ratio (E:T) tested when PLK1 activity was inhibited (Fig.6A). Similar results were obtained using PLK1 KD CTLs (Fig.6B). Hence PLK1 contributes to CTL-mediated killing through its ability to regulate IS assembly.

Discussion

The role of mitotic kinases in non-cycling cells has been as yet poorly investigated. Here we show that PLK1, known to regulate centrosome duplication and microtubule dynamics during mitosis (Joukov and De Nicolo, 2018), is required for IS assembly in non-cycling T cells. We provide evidence that PLK1 subserves a dual role in this process, participating in the TCR signaling cascade and modulating microtubule dynamics. Both these functions converge on centrosome polarization towards the T cell contact with its cognate target, a key step in the formation of a functional IS. In CTLs, the failure of the centrosome to polarize to the IS following pharmacological inhibition or silencing of PLK1 led to impaired LG translocation towards the target cell and defective target cell killing, identifying PLK1 as a new regulator of CTL function.

Key players in early TCR signaling, including the kinases Lck and ZAP-70 and the adaptors LAT and SLP-76, are required for centrosome polarization (Kuhné et al., 2003; Lowin-Kropf et al., 1998). How these early events translate into the physical movement of the centrosome towards the subsynaptic region has been in part elucidated. Diacylglycerol locally produced at the IS by PLCγ acts as a polarity cue for the centrosome through the recruitment of members of the novel and atypical PKC subfamilies (Huse, 2012). TCR signaling also promotes the synaptic recruitment of the dynein-dynactin complex that has been proposed to provide pulling forces on the microtubules radiating from the centrosome (Liu et al., 2013). Additionally, actin filaments that polymerize at the IS periphery interact with these microtubules to provide tension for centrosome translocation (Calvo and Izquierdo, 2021). The mechanism linking the novel and atypical PKCs to the cytoskeletal elements that provide the pulling forces remains to be fully characterized. The implication of PLK1 in TCR signaling, starting with the activation of the initiating kinase Lck, is likely to account, at least in part, for the defect in centrosome polarization observed in PLK1-inhibited or -depleted T cells. The TCR-dependent recruitment of a pool of phosphorylated PLK1 to the IS places it in a strategic position to regulate the early signaling events that orchestrate centrosome polarization.

How PLK1 regulates the activity of Lck remains to be determined. The activity of Lck is tightly controlled by the phosphorylation status of Y394 and Y505. While full activation requires Y505 dephosphorylation by the transmembrane tyrosine phosphatase CD45 and Y394

autophosphorylation, serine phosphorylation contributes to fine-tuning its activity (Rossy et al., 2012). The threonine/serine kinase Erk has been shown to phosphorylate Lck on S59 under conditions of strong TCR stimulation, which prevents the recruitment of the phosphatase SHP-1 that disables Lck by dephosphorylating Y394, thereby sustaining TCR signaling (Štefanová et al., 2003). PLK1 could be hypothesized to participate directly or indirectly in such regulatory circuitry. As the search for PLK1 substrates has been mainly restricted to the context of mitosis, extending these studies to non-cycling cells may provide new insights into the non-mitotic functions of this kinase.

In mitotic cells PLK1 regulates microtubule dynamics by promoting microtubule nucleation at the centrosome through phosphorylation of PCM components, such as SPD-5 in *C. elegans*, that recruit the γ-tubulin ring complex (γ-TuRC) (Ohta et al., 2021). Additionally, PLK1 regulates microtubule-based microtubule nucleation in human cells during mitotic spindle formation by promoting the interaction of the γ-TuRC recruitment protein, Nedd1, with microtubule-bound Augmin (Johmura et al., 2011). PLK1 has also been implicated in the control of microtubule stability in *D. melanogaster* and mammalian cells through its ability to modulate the activity of the microtubule-associated protein CLASP and the (+) end microtubule motor Kif13 (Moriwaki and Goshima, 2016). Consistent with a role for PLK1 in microtubule dynamics, the rate and extent of microtubule growth has been shown to decrease in PLK1-inhibited human breast adenocarcinoma MCF-7 cells, concomitant with an increase in microtubule acetylation (Rashid et al., 2020). Microtubule dynamics is essential for centrosome polarization to the IS. Genetic depletion of regulators of microtubule growth or stability in T cells, such as the microtubule-binding proteins EB1 and stathmin (Filbert et al., 2012; Martín-Cófreces et al., 2012; Zyss et al., 2011) or modulation of tubulin acetylation through HDAC6 overexpression (Serrador et al., 2004), have been associated with impairment or delay in centrosome polarization to the IS and defective T cell function. It is noteworthy that, while faster rates of microtubule growth translate to increased traction forces that improve the killing activity of CTLs (Pathni et al., 2022), microtubule overgrowth, as observed in T cells depleted of the kinesin Kif21B, also leads to a similar defect (Hooikaas et al., 2020), underscoring the notion that microtubule dynamics must be tightly controlled during the complex process of centrosome translocation to the IS and the subsequent polymerization of new microtubules from the repositioned centrosome. Our finding that PLK1 regulates microtubule growth during IS assembly suggests that its ability to promote centrosome polarization might not be limited to its role in TCR signaling but also

depend on a more direct role in microtubule nucleation at the centrosome. Interestingly, the *Xenopus* Polo-like kinase Plx1 has been reported to regulate the function of stathmin/Op18 (Budde et al., 2001). Additionally, in pre-mitotic ciliated cells PLK1 promotes cilium disassembly by phosphorylating HDAC6, thereby promoting microtubule deacetylation and disassembly (Wang et al., 2013). The finding that EB1, stathmin and HDAC6 are recruited to the IS in T cells (Filbert et al., 2012; Martín-Cófreces et al., 2012; Serrador et al., 2004) provides a potential direct link between PLK1 and microtubule dynamics during IS assembly.

It is noteworthy that the effects of PLK1 inhibition or depletion in T cells reported here do not completely phenocopy the effects elicited by blockade or depletion of its upstream regulator AurA in $CD4^+$ T cells (Blas-Rus et al., 2016). Both associate with the T cell centrosome and localize at the IS, where a pool of either active kinase can be found. They are both required for Lck activation and early TCR signaling and for microtubule growth during IS formation. However, a major difference is in their ability to promote centrosome translocation, which is not affected in AurA-targeted T cells (Blas-Rus et al., 2016). While the study on AurA was carried out on freshly purified $CD4^+$ T cells and our study mainly on $CD8^+$ cells differentiated to CTLs, we found a similar inhibitory effect of PLK1 blockade on centrosome polarization to the IS in freshly purified $CD4^+$ T cells, as well as in the $CD4^+$ T cell-derived Jurkat cell line. This suggests that, while the AurA/PLK1 axis that regulates mitosis is operational during IS assembly in non-cycling T cells, PLK1 does not only act as effector of AurA but also subserves AurA-independent functions in this process.

Not surprisingly considering its key role in cell division, PLK1 is overexpressed in many types of both solid and blood cancers (Iliaki et al., 2021). A plethora of studies have provided evidence that targeting PLK1 using selective pharmacological inhibitors blocks the proliferation of cancer cells and promotes their apoptosis, setting the basis for a number of clinical trials (Gutteridge et al., 2016; Park et al., 2015; Strebhardt, 2010; Su et al., 2022; Zeidan et al., 2020). Our finding that PLK1 is required for IS assembly, on which T cell activation depends, highlights a potential drawback of PLK1-targeted therapies. The T cell suppressive activity of a PLK1-specific inhibitor on the activation of alloreactive T cells in acute graft-versus-host disease (Hooikaas et al., 2020), while highlighting the potential therapeutic benefits of targeting PLK1 in this disease context, underscores the importance of investigating the immune functions of cancer patients undergoing PLK1-directed therapies.

Materials and methods

Cells, T cell transfectants, antibodies

$CD8^+$ and $CD4^+$ T cells were isolated from peripheral blood of anonymous healthy donors obtained from the Siena University Hospital blood bank. The study was approved by the local ethics committee (Siena University Hospital). Informed consent was obtained from blood donors by the physician in charge of the Siena University Hospital blood bank. Samples were anonymized before distribution. Primary $CD8^+$ and $CD4^+$ T cells were isolated by negative selection through either RosetteSep™ Human $CD8^+$ T Cell Enrichment Cocktail (StemCell technologies, Vancouver, Canada) or RosetteSep™ Human $CD4^+$ T Cell Enrichment Cocktail (StemCell technologies, Vancouver, Canada) and centrifugation over a buoyant density medium (Lympholyte Cell Separation Medium, Euroclone, Milan, Italy). Immediately after isolation, $CD8^+$ and $CD4^+$ T cells were resuspended in RPMI 1640 with 25 mM Hepes (Sigma-Aldrich, St. Louis, Missouri, USA), supplemented with 10% BCS (Bovine Calf Serum, Hyclone, Logan, Utah, USA) inactivated at 56 °C for 30 minutes, 20 U/mL Penicillin (Sigma-Adrich, St. Louis, Missouri, USA) and 1X non-essential amino acids (MEM non-essential amino acids solution 100X, Gibco, Waltham, Massachusetts, USA). Cell cultures were maintained at 37 °C and 5% CO_2. Freshly isolated $CD8^+$ T cells were differentiated *in vitro* to CTLs by incubation for 48 h with anti-CD3/CD28 coated magnetic beads (Dynabeads Human T-activator CD3/CD28, Gibco, Waltham, Massachusetts, USA) for cell expansion and activation and 50 U/mL of IL-2 (human Interleukin-2, Miltenyi Biotech, Bergisch Gladbach, Germany) for cell proliferation and differentiation. Mature CTLs (days 5 to 7 of differentiation) were used for the experiments (Onnis *et al.*, 2022). Freshly isolated $CD4^+$ T cells were immediately used for the assays.

To generate CTL clones, $CD8^+$ T cells specific for the VLAELVKQI peptide of the cytomegalovirus protein pp65 were single cell sorted into 96-U-bottom plates using a BD FACSAria II cell sorter using tetramer staining. Cells were cultured in RPMI 1640 medium supplemented with 8% human AB serum (PAA), minimum essential amino acids, HEPES and sodium pyruvate (Invitrogen), 100 IU/ml human rIL-2 and 50 ng/ml human rIL-15. $CD8^+$ T-cell clones were stimulated in complete RPMI/HS medium containing 1 mg/ml PHA with 1 x 10^6/ ml 35 Gy irradiated allogeneic peripheral blood mononuclear cells (isolated on Ficoll Paque Gradient from buffy coats of healthy donors) and 1 x 10^5/ ml 70 Gy irradiated EBV-transformed B cells. Re-stimulation of clones was performed every 2 weeks. Blood samples were collected and processed following standard ethical procedures (Helsinki protocol),

after obtaining written informed consent from each donor and approval for this study by the local ethical committee (Comité de Protection des Personnes Sud-Ouest et Outremer II). Other cells used were Raji B cells, EBV-transformed B cells (JY) and Jurkat T cells (ATCC, Manassas, VA), maintained in RPMI 1640 supplemented with 7.5% BCS and 20 U/ml Penicillin.

For RNAi-mediated PLK1 silencing CTLs were transiently transfected at day 6 of differentiation using the Human T cell nucleofector kit and the program T-023 of the Nucleofector II system (Amaxa Biosystems, Euroclone, Milan, Italy) for activated cells with human PLK1-specific siRNAs (#4390824, s448) and negative control siRNA (#4390846) (Invitrogen, Waltham, Massachusetts, USA) (150 ng/10^6 cells). Cells were used 24 h post-transfection. All samples were tested by immunoblotting to check the efficiency of PLK1 knockdown.

CTLs were transiently transfected with the pEGFP plasmid encoding the EB1-GFP fusion protein (Addgene #17234, Watertown, Massachusetts, USA). Briefly, CTLs at 5 days of differentiation were transiently transfected using the Human T cell nucleofector kit and the program T-023 of the Nucleofector II system (Amaxa Biosystems, Euroclone, Milan, Italy) for activated cells with 1 μg/10^6 cells of pEGFP-EB1 plasmid. Transfected cells were gently resuspended in the culture medium added with 500 U/ml IL-2 and analysed 24 h post-transfection.

T cells were pre-treated with the PLK inhibitor BI2536 (Selleckchem, Houston, Texas, USA) at the concentration of 100 nM in DMSO in serum-free medium for 3 h at 37°C and 5% CO_2 and used as such for the assays (Lénárt et al., 2007). Control samples were incubated with the same amount of DMSO.

All primary commercial antibodies used in the assays are listed in Table 1, together with information on the dilutions used for immunoblotting and immunofluorescence. Secondary horseradish peroxidase (HRP)-labelled antibodies were purchased from Jackson ImmunoResearch Laboratories (West Grove, Pennsylvania, USA) and Alexa Fluor 488- and 555-labeled secondary antibodies from ThermoFisher Scientific (Waltham, Massachusetts, USA). IgG from OKT3 (anti-human CD3ε, IgG2) hybridoma supernatants was purified using Mabtrap (Amersham Biosciences, Inc., Piscataway, NJ, USA) and titrated by flow cytometry.

Conjugate formation, CTL activation on activating surfaces, immunofluorescence and image analysis

Conjugates between CD8$^+$ T cells and superantigen-pulsed Raji B cells were carried out as previously described (Cassioli et al., 2021). Raji B cells (used as APCs) were loaded with 10 μg/ml of a mix of Staphylococcal Enterotoxins A (SEA), B (SEB) and E (SEE) (Toxin Technologies, Sarasota, Florida, USA) for 2 h at 37°C and labelled with 10 μM Cell Tracker Blue for the last 20 min of the incubation with superantigens (SAgs). Conjugates of CTLs with unpulsed Raji B cells were used as negative controls. SAg-pulsed or unpulsed Raji B cells were mixed with CTLs (1:1) to allow conjugate formation at 37°C for the indicated time points. Samples were seeded onto poly-L-lysine (Merck, Drmstadt, Germany)-coated slides (ThermoFisher Scientific, Waltham, Massachusetts, USA). Alternatively, CTLs were activated in the absence of target cells by plating on 5 μg/ml anti-CD3 antibody (clone OKT3)(Bio Legend, San Diego, California, USA)-coated slides. Cells were fixed with either methanol at -20°C for 10 min or 4% paraformaldehyde/PBS at room temperature for 15 min. After washing with PBS, cells were stained with primary antibodies at 4°C overnight, and then incubated at room temperature for 45 min with Alexa fluor 488- and 555-labeled secondary antibodies and mounted with 90% glycerol/PBS.

Confocal microscopy was carried out on a Zeiss LSM700 microscope (Carl Zeiss, Jena, Germany) using a 63x/1.40 oil immersion objective or a spinning disk confocal and super-resolution microscope (CSU-W1-SoRA Nikon), with 100x/1.49 oil objective. 3D deconvolution (Blind method, 20 iterations) and denoise were performed using the software NIS Elements AR Nikon and applied to high-resolution images. Detectors were set to detect the optimal signal below the saturation limits.

Co-localization analyses were performed on medial optical sections of single cells using ImageJ and the JACoP plugin to calculate Mander's coefficient (Manders et al., 1992). Mander's coefficients range from 0 to 1, corresponding to non-overlapping images and 100% co-localization between both images, respectively.

Polarization of CD3ζ, GzmB$^+$ lytic granules and PLK1, and the translocation of the centrosome to the IS, were based on the presence of the staining solely on the CTL:APC contact site and were expressed as the percentage of conjugates with synaptic staining *versus* the total number of conjugates analysed. The relative distance of the centrosome, PLK1, AurA and individual GzmB$^+$ vesicles from the contact site of CTLs with APCs or individual GzmB$^+$ vesicles from the centrosome was measured using ImageJ. The recruitment index was calculated as the ratio of either CD3ζ or pPLK1 fluorescence intensity at the synaptic area, which is manually defined at the CTL:APC contact site *versus* the entire cell membrane, using ImageJ. The relative pPLK1 fluorescence at the centrosome was

calculated over a circular region defined from the point of PCM1 maximal intensity. The skewness of the intensity distribution of α-tubulin was measured using Fiji, by calculating the mean value of 3 different regions (2x3 μm) for each cell, excluding the centrosomal area.

Live cell imaging and analysis

For TIRF microscopy, EB1-EGFP transfected CTLs were washed and seeded at 1.5 x 10^5 cells per well on 5 μg/ml anti-CD3 antibody (clone OKT3)-coated eight-well chambered slides (Ibidi, Munich, Germany). Chambered slides were mounted on a heated stage within a temperature-controlled chamber maintained at 37 °C, and constant CO_2 concentrations (5%). Cells were visualized using a CSU-W1-SoRA Nikon microscope coupled to Photometrics BSI (Nikon) camera fitted with 100x/1.49 oil objective. Images were taken every 300 ms for 3 minutes and time lapses were processed with the confocal software NIS Elements AR Nikon. Images were equalized in intensity in time, denoised, background corrected and then bright spots were detected and tracked.

Cell lysis and Immunoblotting

Cells (2x10^6/sample) were stimulated with purified anti-human CD3ε for the indicated time at 37°. Cells were then lysed in 0.5% (v/v) Triton X-100 in 20 mM Tris–HCl (pH 8), 150 mM NaCl in the presence of Protease inhibitor Cocktail Set III (Calbiochem®, Merck, Darmstadt, Germany) and the phosphatase inhibitor sodium orthovanadate (Sigma-Aldrich, St. Louis, Missouri, USA) for 5 min on ice. Protein extracts from post-nuclear supernatants were quantified with the Quantum protein assay kit (Euroclone, Milan, Italy) and denatured in 4x Bolt SDS sample buffer (Invitrogen, Waltham, Massachusetts, USA) supplemented with 10x Bolt sample reducing buffer (Invitrogen, Waltham, Massachusetts, USA) for 5 min at 100°C. Proteins (10 μg) were subjected to SDS-PAGE on Bolt Bis-Tris mini protein gels (Invitrogen, Waltham, Massachusetts, USA) and transferred to nitrocellulose (GE HealthCare, Euroclone, Milan, Italy) under wet conditions. Blocking was performed in 5% non-fat dry milk in PBS containing 0.2% Tween 20 (Sigma-Aldrich, St. Louis, Missouri, USA). Membranes were incubated in primary antibodies for 1-3 h at room temperature (20-25°C) or overnight at 4°C, followed by incubation with 20 ng/ml HRP-conjugated secondary antibodies (Jackson ImmunoResearch Laboratories, West Grove, Pennsylvania, USA) for 45 min at room temperature. Secondary antibodies were detected using SuperSignal west pico plus chemiluminescent substrate (Life Technologies, Waltham, Massachusetts, USA). For quantification, immunoblot membranes were scanned using Alliance Q9-Atom

chemiluminescence imaging system (Uvitec, Cambridge, UK), and densitometric levels were measured using ImageJ software (National Institutes of Health, USA).

Real-time calcein release-based killing assay

Raji B cells were loaded with 500 nM calcein-AM (Life Technology, Waltham, Massachusetts, USA) in AIM V medium (ThermoFisher Scientific, Waltham, Massachusetts, USA) with 10 mM Hepes at room temperature for 15 min, washed and plated in 96-well black plates with clear bottom (BD Falcon, Corning, New York, USA). BI2536-treated or PLK1 KD CTLs and controls were added at different ratios to $0.5x10^4$ settled target cells per well to measure killing at 37°C, 5% CO_2. Triton X-100 (1%) was added to target cells alone to calculate maximal target cell lysis as control. Target cell lysis was measured every 10 min for 4 h. The decreased calcein fluorescence in target cells due to cell lysis was measured at 485 nm excitation wavelength and 528 nm emission wavelength in the bottom reading mode using a Synergy HTX multi-mode plate reader (BioTek, Santa Clara, California, USA). The fluorescence for the experimental condition was adjusted by the parameter γ according to the live target cell control fluorescence. The γ value was measured at time zero: $\gamma = F_{live}(0)/F_{exp}(0)$. Cytotoxicity was calculated based on the loss of calcein fluorescence in target cells using the equation: % target cell lysis = $(F_{live} - \gamma \times F_{exp})/(F_{live}-F_{lyse}) \times 100$, where F_{live} is the fluorescence of target cells alone, F_{exp} are CTL+APC samples and F_{lyse} is the maximal target cell lysis. All the experiments were performed in duplicate and averaged to obtain one dataset. The maximal CTL-induced target cell killing was assigned to the higher CTL:APC ratio, on which the relative values for the other samples were based (Chang et al., 2018).

Statistics and reproducibility

Each experiment is the result of at least 3 independent replicates. The number of cells analysed is specified in the figure legends. Statistical analyses were performed using Prism software (GraphPad Software). Pairwise or multiple comparisons of values with normal distribution were carried out using Student's t-test (unpaired), one-sample t-test (theoretical mean=1) and one-way ANOVA, whereas values without Gaussian distribution were analysed with Mann-Whitney test or Kruskal-Wallis test. Statistical significance was defined as: ****P≤0.0001; ***P≤0.001; **P≤0.01; *P≤0.05; n.s., not significant.

549 **Table T1. List of the primary antibodies used in this work**

550

Antibody (anti-)	Host species	Company	Catalog number	Dilution WB	Dilution IF
Actin	mouse	Millipore (Burlington, Massachusetts, USA)	MAB1501	1:10,000	-
Aurora-A	rabbit	Cell signalling (Danvers, Massachusetts, USA)	14475	-	1:100
CD3ζ	mouse	Santa Cruz (California, USA)	sc-1239	-	1:200
pErk1/2 (T202/Y204)	rabbit	Cell signalling (Danvers, Massachusetts, USA)	9101	1:1,000	-
Granzyme B-488	mouse	Bio Legend (San Diego, California, USA)	560211	-	1:20
pLat (Y191)	rabbit	Cell signalling (Danvers, Massachusetts, USA)	3584S	1:1,000	-
Lck	mouse	BD (Franklin Lakes, New Jersey, USA)	610097	-	1:50
pLck (Y394)	mouse	Bio-techne (Minneapolis, Minnesota, USA)	MAB7500	1:1000	1:50

PCM1	mouse	Santa Cruz (California, USA)	sc-398365	-	1:300
Pericentrin	rabbit	Abcam (Cambridge, UK)	ab4448	-	1:200
PLK1	rabbit	Bio-techne (Minneapolis, Minnesota, USA)	104302	1:500	1:300
pPLK1 (S137)	rabbit	Abcam (Cambridge, UK)	ab21738	1:1,000	1:300
α-tubulin	mouse	Santa Cruz (California, USA)	sc-32293	-	1:500
γ-tubulin	mouse	Sigma-Aldrich (St. Louis, Missouri, USA)	T6557	-	1:200

551

Acknowledgements

The authors wish to thank Giuliano Callaini for critical reading of the manuscript and Annamaria Fusillo for technical assistance.

Competing interests

The authors declare no competing financial interests.

Funding

This research has received funding from the European Commission (ERC_2021_SyG 951329 - ATTACK) to CTB and SV and AIRC (IG 2017-20148) to CTB.

Data availability

Data generated in this study are available upon request from corresponding author FF.

References

Andrés-Delgado, L., Antón, O.M., Alonso, M.A., 2013. Centrosome Polarization in T Cells: A Task for Formins. Front. Immunol. 4. https://doi.org/10.3389/fimmu.2013.00191

Bálint, Š., Müller, S., Fischer, R., Kessler, B.M., Harkiolaki, M., Valitutti, S., Dustin, M.L., 2020. Supramolecular attack particles are autonomous killing entities released from cytotoxic T cells. Science 368, 897-901. https://doi.org/10.1126/science.aay9207.

Banerjee, P.P., Pandey, R., Zheng, R., Suhoski, M.M., Monaco-Shawver, L., Orange, J.S., 2007. Cdc42-interacting protein–4 functionally links actin and microtubule networks at the cytolytic NK cell immunological synapse. J. Exp. Med. 204, 2305–2320. https://doi.org/10.1084/jem.20061893

Bertrand, F., Müller, S., Roh, K.-H., Laurent, C., Dupré, L., Valitutti, S., 2013. An initial and rapid step of lytic granule secretion precedes microtubule organizing center polarization at the cytotoxic T lymphocyte/target cell synapse. Proc. Natl. Acad. Sci. U.S.A. 110, 6073–6078. https://doi.org/10.1073/pnas.1218640110

Bischoff, J.R., 1998. A homologue of Drosophila aurora kinase is oncogenic and amplified in human colorectal cancers. EMBO J 17, 3052–3065. https://doi.org/10.1093/emboj/17.11.3052

Blas-Rus, N., Bustos-Morán, E., Pérez De Castro, I., De Cárcer, G., Borroto, A., Camafeita, E., Jorge, I., Vázquez, J., Alarcón, B., Malumbres, M., Martín-Cófreces, N.B., Sánchez-Madrid, F., 2016. Aurora A drives early signalling and vesicle dynamics during T-cell activation. Nat Commun 7, 11389. https://doi.org/10.1038/ncomms11389

Bouchet, J., Del Río-Iñiguez, I., Lasserre, R., Agüera-Gonzalez, S., Cuche, C., Danckaert, A., McCaffrey, M.W., Di Bartolo, V., Alcover, A., 2016. Rac1-Rab11- FIP 3 regulatory hub coordinates vesicle traffic with actin remodeling and T-cell activation. EMBO J 35, 1160–1174. https://doi.org/10.15252/embj.201593274

598 Bruinsma, W., Macůrek, L., Freire, R., Lindqvist, A., Medema, R.H., 2013. Bora and Aurora-
599 A continue to activate Plk1 in mitosis. J. Cell Sci. jcs.137216.
600 https://doi.org/10.1242/jcs.137216
601
602 Budde, P.P., Kumagai, A., Dunphy, W.G., Heald, R., 2001. Regulation of Op18 during
603 Spindle Assembly in Xenopus Egg Extracts. J. Cell Biol. 153, 149–158.
604 https://doi.org/10.1083/jcb.153.1.149
605
606 Bunnell, S.C., Hong, D.I., Kardon, J.R., Yamazaki, T., McGlade, C.J., Barr, V.A., Samelson,
607 L.E., 2002. T cell receptor ligation induces the formation of dynamically regulated signaling
608 assemblies. J. Cell Biol. 158, 1263–1275. https://doi.org/10.1083/jcb.200203043
609
610 Calvo, V., Izquierdo, M., 2021. Role of Actin Cytoskeleton Reorganization in Polarized
611 Secretory Traffic at the Immunological Synapse. Front. Cell Dev. Biol. 9, 629097.
612 https://doi.org/10.3389/fcell.2021.629097
613
614 Cassioli, C., Baldari, C.T., 2022. The Expanding Arsenal of Cytotoxic T Cells. Front.
615 Immunol. 13, 883010. https://doi.org/10.3389/fimmu.2022.883010
616
617 Cassioli, C., Onnis, A., Finetti, F., Capitani, N., Brunetti, J., Compeer, E.B., Niederlova, V.,
618 Stepanek, O., Dustin, M.L., Baldari, C.T., 2021. The Bardet–Biedl syndrome complex
619 component BBS1 controls T cell polarity during immune synapse assembly. J. Cell Sci. 134,
620 jcs258462. https://doi.org/10.1242/jcs.258462
621
622 Chang, H.-F., Mannebach, S., Beck, A., Ravichandran, K., Krause, E., Frohnweiler, K.,
623 Fecher-Trost, C., Schirra, C., Pattu, V., Flockerzi, V., Rettig, J., 2018. Cytotoxic granule
624 endocytosis depends on the Flower protein. J. Cell Biol. 217, 667–683.
625 https://doi.org/10.1083/jcb.201706053
626
627 Chang, H.F., Schirra, C., Ninov, M., Hahn, U., Ravichandran, K., Krause, E., Becherer, U.,
628 Bálint, Š., Harkiolaki, M., Urlaub, H., Valitutti, S., Baldari, C.T., Dustin, M.L., Jahn, R., Rettig,
629 J., 2022. Identification of distinct cytotoxic granules as the origin of supramolecular attack
630 particles in T lymphocytes. Nat. Commun. 13, 1029. https://doi.org/10.1038/s41467-022-
631 28596-y.

Colicino, E.G., Hehnly, H., 2018. Regulating a key mitotic regulator, polo-like kinase 1 (PLK1). Cytoskeleton 75, 481–494. https://doi.org/10.1002/cm.21504

Das, V., Thoulouze, M.-I., Galli, T., Roux, P., Dautry-Varsat, A., Alcover, A., 2004. Activation-Induced Polarized Recycling Targets T Cell Antigen Receptors to the Immunological Synapse: Involvement of SNARE Complexes. Immunity 20, 577-588.

De La Roche, M., Asano, Y., Griffiths, G.M., 2016. Origins of the cytolytic synapse. Nat. Rev. Immunol. 16, 421–432. https://doi.org/10.1038/nri.2016.54

De La Roche, M., Ritter, A.T., Angus, K.L., Dinsmore, C., Earnshaw, C.H., Reiter, J.F., Griffiths, G.M., 2013. Hedgehog Signaling Controls T Cell Killing at the Immunological Synapse. Science 342, 1247–1250. https://doi.org/10.1126/science.1244689

Dixit, R., Ross, J.L., 2010. Studying Plus-End Tracking at Single Molecule Resolution Using TIRF Microscopy, in: Methods in Cell Biology. Elsevier, pp. 543–554. https://doi.org/10.1016/S0091-679X(10)95027-9

Douanne, T., Griffiths, G.M., 2021. Cytoskeletal control of the secretory immune synapse. Curr. Opin. Cell Biol. 71, 87–94. https://doi.org/10.1016/j.ceb.2021.02.008

Filbert, E.L., Le Borgne, M., Lin, J., Heuser, J.E., Shaw, A.S., 2012. Stathmin Regulates Microtubule Dynamics and Microtubule Organizing Center Polarization in Activated T Cells. J. Immunol. 188, 5421–5427. https://doi.org/10.4049/jimmunol.1200242

Gomez, T.S., Billadeau, D.D., 2008. T Cell Activation and the Cytoskeleton: You Can't Have One Without the Other, in: Advances in Immunology. Elsevier, pp. 1–64. https://doi.org/10.1016/S0065-2776(08)00001-1.

Gorman, J.A., Babich, A., Dick, C.J., Schoon, R.A., Koenig, A., Gomez, T.S., Burkhardt, J.K., Billadeau, D.D., 2012. The Cytoskeletal Adaptor Protein IQGAP1 Regulates TCR-Mediated Signaling and Filamentous Actin Dynamics. J. Immunol. 188, 6135–6144. https://doi.org/10.4049/jimmunol.1103487

Green, D.R., Llambi F., 2015. Cell Death Signaling. Cold Spring Harb. Perspect. Biol. 7, a006080. https://doi.org/ 10.1101/cshperspect.a006080

Gutteridge, R.E.A., Ndiaye, M.A., Liu, X., Ahmad, N., 2016. Plk1 Inhibitors in Cancer Therapy: From Laboratory to Clinics. Mol. Cancer Ther. 15, 1427–1435. https://doi.org/10.1158/1535-7163.MCT-15-0897

Higaki, T., Kutsuna, N., Sano, T., Kondo, N., Hasezawa, S., 2010. Quantification and cluster analysis of actin cytoskeletal structures in plant cells: role of actin bundling in stomatal movement during diurnal cycles in Arabidopsis guard cells. Plant J. 61, 156–165. https://doi.org/10.1111/j.1365-313X.2009.04032.x

Higaki, T., 2017. Quantitative evaluation of cytoskeletal organizations by microscopic image analysis. Plant Morphol. 29, 15–21. https://doi.org/10.5685/plmorphol.29.15

Hooikaas, P.J., Damstra, H.G., Gros, O.J., Van Riel, W.E., Martin, M., Smits, Y.T., Van Loosdregt, J., Kapitein, L.C., Berger, F., Akhmanova, A., 2020. Kinesin-4 KIF21B limits microtubule growth to allow rapid centrosome polarization in T cells. eLife 9, e62876. https://doi.org/10.7554/eLife.62876

Huse, M., 2012. Microtubule-organizing center polarity and the immunological synapse: protein kinase C and beyond. Front. Immun. 3. https://doi.org/10.3389/fimmu.2012.00235

Huse, M., Le Floc'h, A., Liu, X., 2013. From lipid second messengers to molecular motors: microtubule-organizing center reorientation in T cells. Immunol. Rev. 256, 95–106. https://doi.org/10.1111/imr.12116

Ilani, T., Khanna, C., Zhou, M., Veenstra, T.D., Bretscher, A., 2007. Immune synapse formation requires ZAP-70 recruitment by ezrin and CD43 removal by moesin. J. Cell Biol. 179, 733–746. https://doi.org/10.1083/jcb.200707199

Iliaki, S., Beyaert, R., Afonina, I.S., 2021. Polo-like kinase 1 (PLK1) signaling in cancer and beyond. Biochem. Pharmacol. 193, 114747. https://doi.org/10.1016/j.bcp.2021.114747

Jenkins, M.R., Stinchcombe, J.C., Au-Yeung, B.B., Asano, Y., Ritter, A.T., Weiss, A., Griffiths, G.M., 2014. Distinct structural and catalytic roles for Zap70 in formation of the immunological synapse in CTL. eLife 3, e01310. https://doi.org/10.7554/eLife.01310

Johmura, Y., Soung, N.-K., Park, J.-E., Yu, L.-R., Zhou, M., Bang, J.K., Kim, B.-Y., Veenstra, T.D., Erikson, R.L., Lee, K.S., 2011. Regulation of microtubule-based microtubule nucleation by mammalian polo-like kinase 1. Proc. Natl. Acad. Sci. U.S.A. 108, 11446–11451. https://doi.org/10.1073/pnas.1106223108

Joukov, V., De Nicolo, A., 2018. Aurora-PLK1 cascades as key signaling modules in the regulation of mitosis. Sci. Signal. 11, eaar4195. https://doi.org/10.1126/scisignal.aar4195

Kabanova, A., Zurli, V., Baldari, C.T., 2018. Signals Controlling Lytic Granule Polarization at the Cytotoxic Immune Synapse. Front. Immunol. 9, 307. https://doi.org/10.3389/fimmu.2018.00307

Kuhn, J.R., Poenie, M., 2002. Dynamic Polarization of the Microtubule Cytoskeleton during CTL-Mediated Killing. Immunity 16, 111–121. https://doi.org/10.1016/S1074-7613(02)00262-5

Kuhné, M.R., Lin, J., Yablonski, D., Mollenauer, M.N., Ehrlich, L.I.R., Huppa, J., Davis, M.M., Weiss, A., 2003. Linker for Activation of T Cells, ζ-Associated Protein-70, and Src Homology 2 Domain-Containing Leukocyte Protein-76 are Required for TCR-Induced Microtubule-Organizing Center Polarization. J. Immunol. 171, 860–866. https://doi.org/10.4049/jimmunol.171.2.860

Lénárt, P., Petronczki, M., Steegmaier, M., Di Fiore, B., Lipp, J.J., Hoffmann, M., Rettig, W.J., Kraut, N., Peters, J.-M., 2007. The Small-Molecule Inhibitor BI 2536 Reveals Novel Insights into Mitotic Roles of Polo-like Kinase 1. Curr. Biol. 17, 304–315. https://doi.org/10.1016/j.cub.2006.12.046

Li, R., Gundersen, G.G., 2008. Beyond polymer polarity: how the cytoskeleton builds a polarized cell. Nat. Rev. Mol. Cell. Biol. 9, 860–873. https://doi.org/10.1038/nrm2522

734 Liu, X., Kapoor, T.M., Chen, J.K., Huse, M., 2013. Diacylglycerol promotes centrosome
735 polarization in T cells via reciprocal localization of dynein and myosin II. Proc. Natl. Acad.
736 Sci. U.S.A. 110, 11976–11981. https://doi.org/10.1073/pnas.1306180110
737
738 Lowin-Kropf, B., Shapiro, V.S., Weiss, A., 1998. Cytoskeletal Polarization of T Cells Is
739 Regulated by an Immunoreceptor Tyrosine-based Activation Motif–dependent Mechanism.
740 J. Cell Biol. 140, 861–871. https://doi.org/10.1083/jcb.140.4.861
741
742 McKenzie, B., Valitutti, S., 2023. Resisting T cell attack: tumor-cell-intrinsic defense and
743 reparation mechanisms. Trends Cancer 9, 198-211. https://d
744 oi.org/10.1016/j.trecan.2022.12.003
745
746 Manders, E.M.M., Stap, J., Brakenhoff, G.J., Driel, R.V., Aten, J.A., 1992. Dynamics of
747 three-dimensional replication patterns during the s-phase, analysed by double labelling of
748 dna and confocal microscopy. J. Cell Sci. 103, 857–862.
749 https://doi.org/10.1242/jcs.103.3.857
750
751 Martín-Cófreces, N.B., Baixauli, F., López, M.J., Gil, D., Monjas, A., Alarcón, B., Sánchez-
752 Madrid, F., 2012a. End-binding protein 1 controls signal propagation from the T cell receptor:
753 EB1 regulates TCR signalling. EMBO J. 31, 4140–4152.
754 https://doi.org/10.1038/emboj.2012.242
755
756 Moriwaki, T., Goshima, G., 2016. Five factors can reconstitute all three phases of
757 microtubule polymerization dynamics. J. Cell Biol. 215, 357–368.
758 https://doi.org/10.1083/jcb.201604118
759
760 Nehlig, A., Molina, A., Rodrigues-Ferreira, S., Honoré, S., Nahmias, C., 2017. Regulation of
761 end-binding protein EB1 in the control of microtubule dynamics. Cell. Mol. Life Sci. 74, 2381–
762 2393. https://doi.org/10.1007/s00018-017-2476-2
763
764 Ohta, M., Zhao, Z., Wu, D., Wang, S., Harrison, J.L., Gómez-Cavazos, J.S., Desai, A.,
765 Oegema, K.F., 2021. Polo-like kinase 1 independently controls microtubule-nucleating
766 capacity and size of the centrosome. J. Cell Biol. 220, e202009083.
767 https://doi.org/10.1083/jcb.202009083

Onnis, A., Andreano, E., Cassioli, C., Finetti, F., Della Bella, C., Staufer, O., Pantano, E., Abbiento, V., Marotta, G., D'Elios, M.M., Rappuoli, R., Baldari, C.T., 2023. SARS-CoV-2 Spike protein suppresses CTL-mediated killing by inhibiting immune synapse assembly. J. Exp. Med. 220, e20220906. https://doi.org/10.1084/jem.20220906

Park, J.-E., Kim, T.-S., Kim, B.Y., Lee, K.S., 2015. Selective blockade of cancer cell proliferation and anchorage-independent growth by Plk1 activity–dependent suicidal inhibition of its polo-box domain. Cell Cycle 14, 3624–3634. https://doi.org/10.1080/15384101.2015.1104435

Pathni, A., Özçelikkale, A., Rey-Suarez, I., Li, L., Davis, S., Rogers, N., Xiao, Z., Upadhyaya, A., 2022. Cytotoxic T Lymphocyte Activation Signals Modulate Cytoskeletal Dynamics and Mechanical Force Generation. Front. Immunol. 13, 779888. https://doi.org/10.3389/fimmu.2022.779888

Rashid, A., Naaz, A., Rai, A., Chatterji, B.P., Panda, D., 2020. Inhibition of polo-like kinase 1 suppresses microtubule dynamics in MCF-7 cells. Mol. Cell. Biochem. 465, 27–36. https://doi.org/10.1007/s11010-019-03664-y

Ritter, A.T., Asano, Y., Stinchcombe, J.C., Dieckmann, N.M.G., Chen, B.-C., Gawden-Bone, C., van Engelenburg, S., Legant, W., Gao, L., Davidson, M.W., Betzig, E., Lippincott-Schwartz, J., Griffiths, G.M., 2015. Actin Depletion Initiates Events Leading to Granule Secretion at the Immunological Synapse. Immunity 42, 864–876. https://doi.org/10.1016/j.immuni.2015.04.013

Rossy, J., Williamson, D.J., Gaus, K., 2012. How does the kinase Lck phosphorylate the T cell receptor? Spatial organization as a regulatory mechanism. Front. Immunol. 3. https://doi.org/10.3389/fimmu.2012.00167

Samelson, L.E., 2002. Signal Transduction Mediated by the T Cell Antigen Receptor: The Role of Adapter Proteins. Annu. Rev. Immunol. 20, 371–394. https://doi.org/10.1146/annurev.immunol.20.092601.111357

802 Sanchez, E., Liu, X., Huse, M., 2019. Actin clearance promotes polarized dynein
803 accumulation at the immunological synapse. PLoS ONE 14, e0210377.
804 https://doi.org/10.1371/journal.pone.0210377
805
806 Sardon, T., Peset, I., Petrova, B., Vernos, I., 2008. Dissecting the role of Aurora A during
807 spindle assembly. EMBO J 27, 2567–2579. https://doi.org/10.1038/emboj.2008.173
808
809 Serrador, J.M., Cabrero, J.R., Sancho, D., Mittelbrunn, M., Urzainqui, A., Sánchez-Madrid,
810 F., 2004. HDAC6 Deacetylase Activity Links the Tubulin Cytoskeleton with Immune Synapse
811 Organization. Immunity 20, 417–428. https://doi.org/10.1016/S1074-7613(04)00078-0
812
813 Soares, H., Lasserre, R., Alcover, A., 2013. Orchestrating cytoskeleton and intracellular
814 vesicle traffic to build functional immunological synapses. Immunol. Rev. 256, 118–132.
815 https://doi.org/10.1111/imr.12110
816
817 Steegmaier, M., Hoffmann, M., Baum, A., Lénárt, P., Petronczki, M., Krššák, M., Gürtler, U.,
818 Garin-Chesa, P., Lieb, S., Quant, J., Grauert, M., Adolf, G.R., Kraut, N., Peters, J.-M., Rettig,
819 W.J., 2007. BI 2536, a Potent and Selective Inhibitor of Polo-like Kinase 1, Inhibits Tumor
820 Growth In Vivo. Curr. Biol. 17, 316–322. https://doi.org/10.1016/j.cub.2006.12.037
821
822 Štefanová, I., Hemmer, B., Vergelli, M., Martin, R., Biddison, W.E., Germain, R.N., 2003.
823 TCR ligand discrimination is enforced by competing ERK positive and SHP-1 negative
824 feedback pathways. Nat. Immunol. 4, 248–254. https://doi.org/10.1038/ni895
825
826 Stinchcombe, J.C., Griffiths, G.M., 2014. Communication, the centrosome and the
827 immunological synapse. Phil. Trans. R. Soc. B 369, 20130463.
828 https://doi.org/10.1098/rstb.2013.0463
829
830 Strebhardt, K., 2010. Multifaceted polo-like kinases: drug targets and antitargets for cancer
831 therapy. Nat. Rev. Drug Discov. 9, 643–660. https://doi.org/10.1038/nrd3184
832
833 Su, S., Chhabra, G., Singh, C.K., Ndiaye, M.A., Ahmad, N., 2022. PLK1 inhibition-based
834 combination therapies for cancer management. Trans. Oncol. 16, 101332.
835 https://doi.org/10.1016/j.tranon.2021.101332

Tsun, A., Qureshi, I., Stinchcombe, J.C., Jenkins, M.R., De La Roche, M., Kleczkowska, J., Zamoyska, R., Griffiths, G.M., 2011. Centrosome docking at the immunological synapse is controlled by Lck signaling. J. Cell Biol. 192, 663–674. https://doi.org/10.1083/jcb.201008140

Wang, G., Chen, Q., Zhang, X., Zhang, B., Zhuo, X., Liu, J., Jiang, Q., Zhang, C., 2013. PCM1 Recruits Plk1 to Pericentriolar Matrix to Promote Primary Cilia Disassembly before Mitotic Entry. J. Cell Sci. jcs.114918. https://doi.org/10.1242/jcs.114918

Zeidan, A.M., Ridinger, M., Lin, T.L., Becker, P.S., Schiller, G.J., Patel, P.A., Spira, A.I., Tsai, M.L., Samuëlsz, E., Silberman, S.L., Erlander, M., Wang, E.S., 2020. A Phase Ib Study of Onvansertib, a Novel Oral PLK1 Inhibitor, in Combination Therapy for Patients with Relapsed or Refractory Acute Myeloid Leukemia. Clin. Cancer Res. 26, 6132–6140. https://doi.org/10.1158/1078-0432.CCR-20-2586

Zitouni, S., Nabais, C., Jana, S.C., Guerrero, A., Bettencourt-Dias, M., 2014. Polo-like kinases: structural variations lead to multiple functions. Nat. Rev. Mol. Cell. Biol. 15, 433–452. https://doi.org/10.1038/nrm3819

Zyss, D., Ebrahimi, H., Gergely, F., 2011. Casein kinase I delta controls centrosome positioning during T cell activation. J. Cell Biol. 195, 781–797. https://doi.org/10.1083/jcb.201106025

Figure legends

Figure 1. PLK1 is recruited to and phosphorylated at the IS in CTLs. (A) Immunoblot analysis with anti-PLK1 antibody of lysates of $CD8^+$ T cells collected at days 0, 5 or 7 following stimulation with anti-CD3/CD28 coated beads. A control anti-actin blot of the stripped filter is shown below. The migration of molecular mass markers is indicated. The quantification of PLK1 in CTL lysates is reported in the graph (n=4, mean fold ± SD; ANOVA). **(B)** Quantification using Mander's coefficient of the weighted colocalization of PLK1 and the centrosome markers PCM1 or γ-tubulin in CTLs (30 cells/sample, n=3; mean fold ± SD). Medial optical sections of representative images are shown. Scale bar: 5 µm. **(C)** Immunofluorescence analysis of PLK1 and PCM1 5 or 15 minutes after conjugate formation of CTLs and SAg-loaded Raji cells. Conjugates formed in the absence of SAgs (no SAgs) were used as negative control. Scale bar: 5 µm. The graphs show the percentage of conjugates with PLK1 polarization at the IS (15 cells/sample, n=3; ANOVA)(left) and the quantification of the distance of PLK1 from the IS membrane (µm)(20 cells/sample, n=3; Kurskall Wallis test)(right), respectively. **(D)** Immunoblot analysis with anti-pPLK1 antibody of lysates of CTLs either unstimulated or stimulated with anti-CD3 mAb for the indicated times. A control anti-actin blot of the stripped filter is shown below. The migration of molecular mass markers is indicated. The quantification of pPLK1 in anti-CD3 mAb-stimulated or unstimulated CTLs is reported in the graph (n=3, mean fold ± SD; one sample t test). **(E)** Immunofluorescence analysis of p-PLK1 and PCM1 5 or 15 minutes after conjugate formation of CTLs and SAg-pulsed Raji B cells. Scale bar: 5 µm. The graphs show the percentage of conjugates harbouring accumulation of the phosphorylated form of PLK1 at the IS region (15 cells/sample, n=3; mean ± SD, ANOVA)(left), the quantification of pPLK1 intensity at the IS membrane *versus* the total cell membrane (center) and the quantification of pPLK1 fluorescence intensity in the centrosome region defined from the point of PCM1 maximal intensity (24 cells/sample, n=3; mean ± SD, Kurskall Wallis test)(right).*P < 0.05; **P < 0.01; ***P < 0.001; ****P < 0.0001.

Figure 2. PLK1 inhibition or depletion impairs TCR clustering at the IS in CTLs. (A) Immunofluorescence analysis of the TCR subunit CD3ζ in 5 or 15 minutes conjugates of control (vehicle) and BI2536-treated CTLs and SAg-loaded Raji cells. Representative images of medial optical sections are shown. Scale bar: 5 µm. The histograms show the quantification of the percentages of conjugates positive for CD3ζ polarization to the IS (top)

and the quantification of the relative CD3ζ fluorescence intensity at the IS (bottom)(20 cells/sample, n≥3; ANOVA). (**B**) Immunoblot analysis of PLK1 in representative matched control (scramble RNAi) and PLK1 KD CTLs, with respective loading control (actin) is shown. The migration of molecular mass markers is indicated. The quantification of PLK1 in CTL lysates is reported in the table (n=3; mean fold ± SD, one sample t test). (**C**) Quantification of the immunofluorescence analysis of 5 or 15 minutes conjugates of control and PLK1 KD CTLs and SAg-loaded Raji cells. The histograms show the percentages of conjugates positive for CD3ζ polarization to the IS (left) and the quantification of the relative CD3ζ fluorescence intensity at the IS (right) (10 cells/sample, n=3; ANOVA). *P < 0.05; **P < 0.01; ***P < 0.001; ****P < 0.0001.

Figure 3. PLK1 inhibition impairs TCR signalling in CTLs. (A) Immunofluorescence analysis of the phosphorylated active form of Lck (Y394) (pLck394) in 5 or 15 minutes conjugates of control (vehicle) or BI2536-treated CTLs and SAg-loaded Raji cells. Representative images of medial optical sections are shown. Scale bar: 5 μm. The histograms show the quantification of the percentages of conjugates positive for pLck394 polarization to the IS (top) and the quantification of the relative pLck394 fluorescence intensity at the IS (bottom) (10 cells/sample, n≥3; ANOVA). **(B,C)** Immunoblot analysis with anti-pLck394 (B), anti-pLAT and anti-pErk1/2 (C) antibodies of lysates of either control or BI2536-treated CTLs, unstimulated or stimulated with anti-CD3 mAb for the indicated times. A control anti-actin blot of the stripped filter is shown below. The migration of molecular mass markers is indicated. The graphs show the quantification of pLck394 (B), pErk1/2 and pLAT (C), respectively (n≥3; mean fold ± SD, one-way ANOVA). *P < 0.05; **P < 0.01; ***P < 0.001; ****P < 0.0001.

Figure 4. PLK1 inhibition impairs centrosome and LG polarization to the IS in CTLs. (A) Immunofluorescence analysis of the centrosomal protein pericentrin (PCNT-1) and the LG component granzyme B (GzmB) in 5 and 15 minutes conjugates of vehicle- and BI2536-treated CTLs and SAg-pulsed Raji cells. Medial optical sections of representative images are shown. Scale bar: 5 μm. (**B,E**) Quantification of the percentages of conjugates positive for PCNT-1 at the IS (left) and of the distance of the centrosome from the synaptic membrane (right) (μm) in conjugates of control or BI2536-treated CTLs and Raji B cells (B) or of control and PLK1 KD CTLs (E). (**C,F**) Quantification of the percentages of conjugates positive for GzmB at the IS (top (C), left (F)) and of the mean distance of single GzmB$^+$

vesicles from the synaptic membrane (bottom (C), right (F)) (μm) in individual conjugates of control or BI2536-treated CTLs (C), or of control and PLK1 KD CTLs (F) and Raji B cells. (**D,G**) Quantification of the mean distance of single GzmB$^+$ vesicles from the centrosome in individual conjugates of control and either BI2536-treated (D) or PLK1 KD (G) CTLs and Raji B cells (μm). Data are reported as mean ± SD. Statistical analysis: B-D: 20 cells/sample, n≥3; E-G: 10 cells/sample, n=3; ANOVA. *P < 0.05; **P < 0.01; ***P < 0.001; ****P < 0.0001.

Figure 5. PLK1 inhibition impairs microtubule dynamics in CTLs. (**A,B**) Immunofluorescence analysis of α-tubulin in control and BI2536-treated CTLs. Representative images of maximum intensity projections of z-stacks are shown. Scale bar: 10 μm. (**A**) The arrowhead points to an example of cell displaying microtubules organized in few and thick α-tubulin-decorated bundles, while the arrow points to a cell showing microtubule bundles originating from the cortical area. The graph shows the percentage of cells displaying thick microtubule bundles (n=3; mean fold ± SD, t test). (**B**) Profiles of fluorescence intensity along a manually-selected line (white bar) in representative control or BI2536 treated CTLs. (**C**) Skewness of α-tubulin intensity distribution in control and BI2536-treated CTLs (≥40 cells from 3 independent experiments; mean fold ± SD, t test). (**D**) Imaging of EB1-EGFP-expressing CTLs, pre-treated with DMSO or BI2536 and plated on anti-CD3/CD28-coated glass-bottom chambers. Representative projections of time lapse are shown (Δt = 45 sec). Images were taken every 300 ms for 3 minutes using a TIRF microscope. Scale bar: 5 μm. (**E**) Representative polar graphs of images in panel D showing the trajectories (left) and the speed (right) of EB1-EGFP-decorated microtubule (+) tips showing, respectively, the projection of object movements (color path length corresponds to track length) and the heading of each object as a color arrow (length corresponds to object speed). The external circle in the polar graphs indicates a distance of 2.8 μm (left) or a speed of 0.8 μm/s (right). (**F**) Quantification of the number (left) and length (center) of segments, and the speed of the growing tracks (right), reported as average value per cell (≥32 cells from 3 independent experiments; mean fold ± SD, t test). *P < 0.05; **P < 0.01; ***P < 0.001; ****P < 0.0001.

Figure 6. PLK1 inhibition impairs CTL-mediated killing. (A,B) Real-time calcein release-based killing assay. CTLs either untreated or pre-treated with BI2536 (A) and control or PLK1 KD CTLs (B), were co-cultured with SAg-loaded Raji B cells at the target:CTL ratios indicated, and target cell killing was measured every 10 minutes for 4 hours as reported in

962 the kinetic graph (left). Quantification of the percentage of target cell death at the endpoint
963 of the procedure (4 h) is shown on the right graph. The data refer to at least three
964 independent experiments performed in duplicate and are reported as mean fold ± SD, with
965 target cell lysis at the highest target:CTL ratio of the control sample set at 100% of
966 cytotoxicity (ANOVA). *P < 0.05; **P < 0.01; ***P < 0.001; ****P < 0.0001.

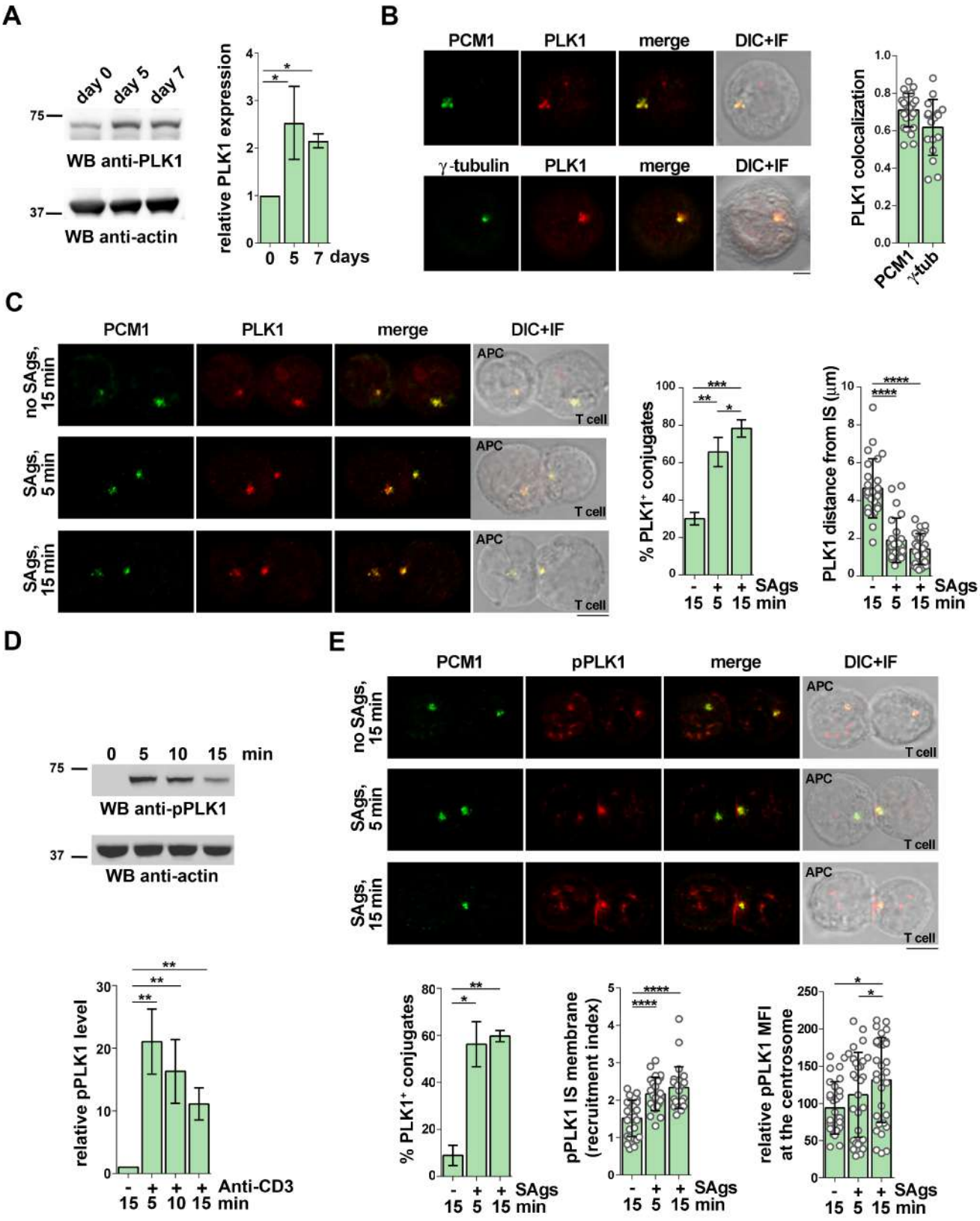

Figure 1

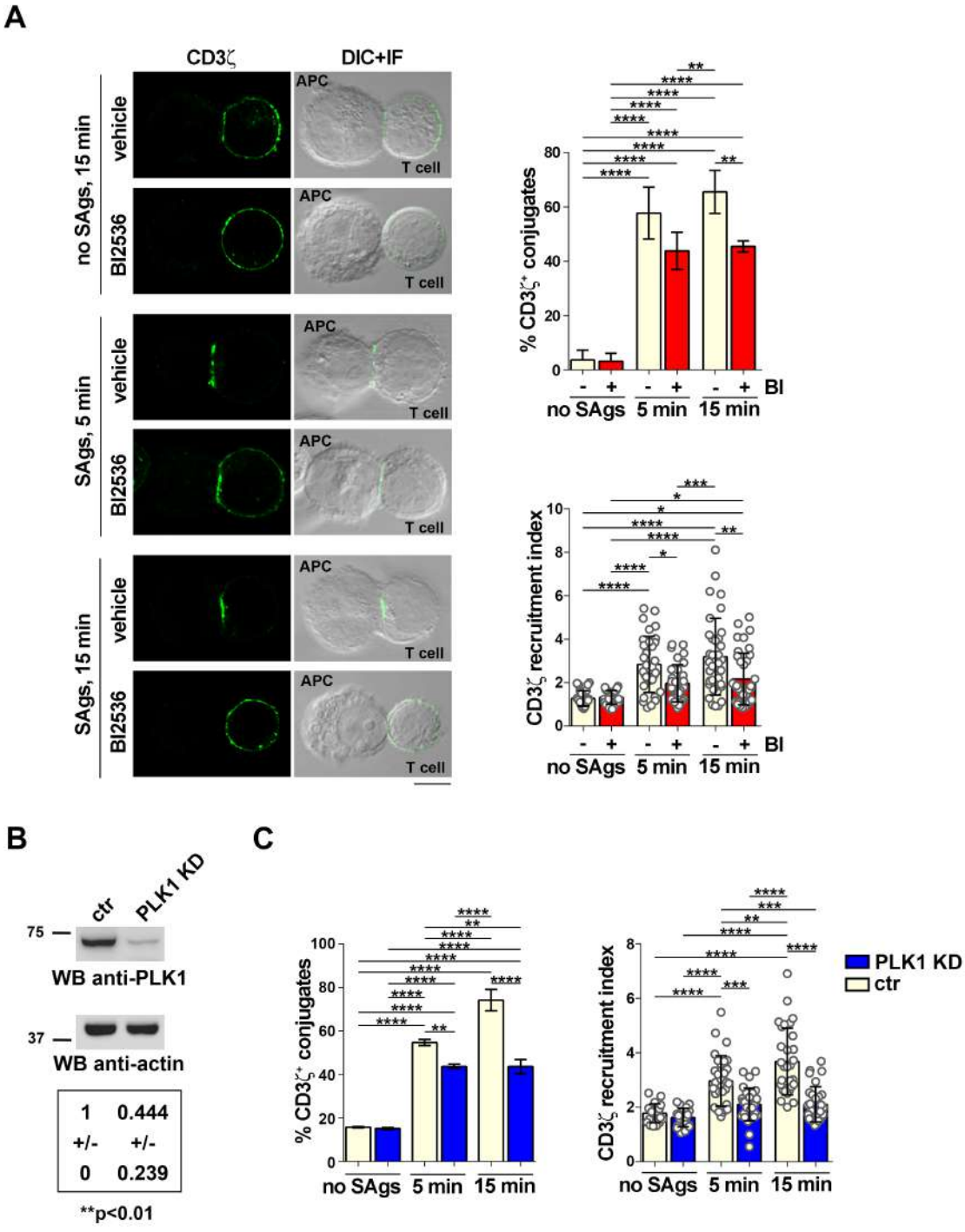

Figure 2

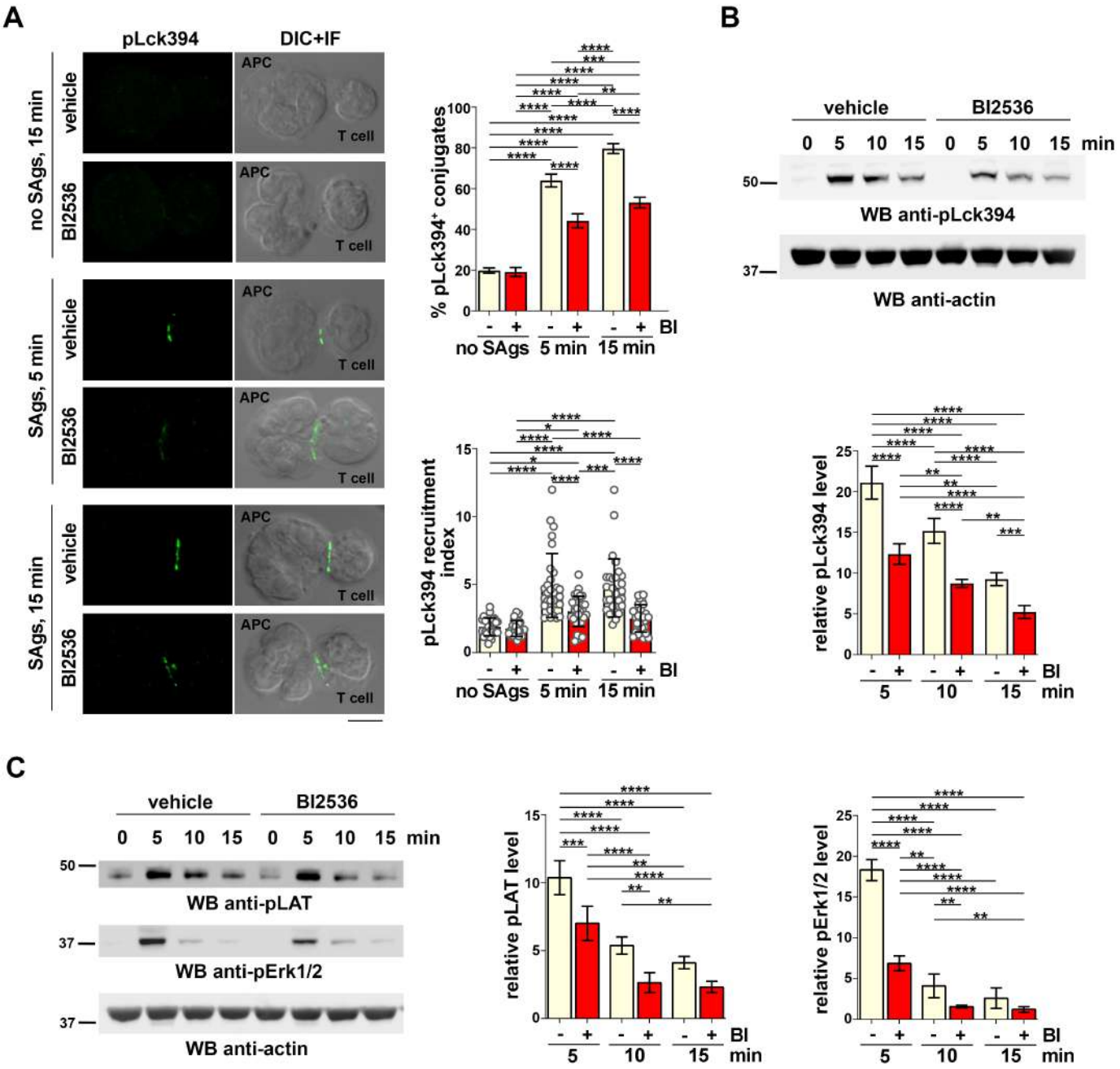

Figure 3

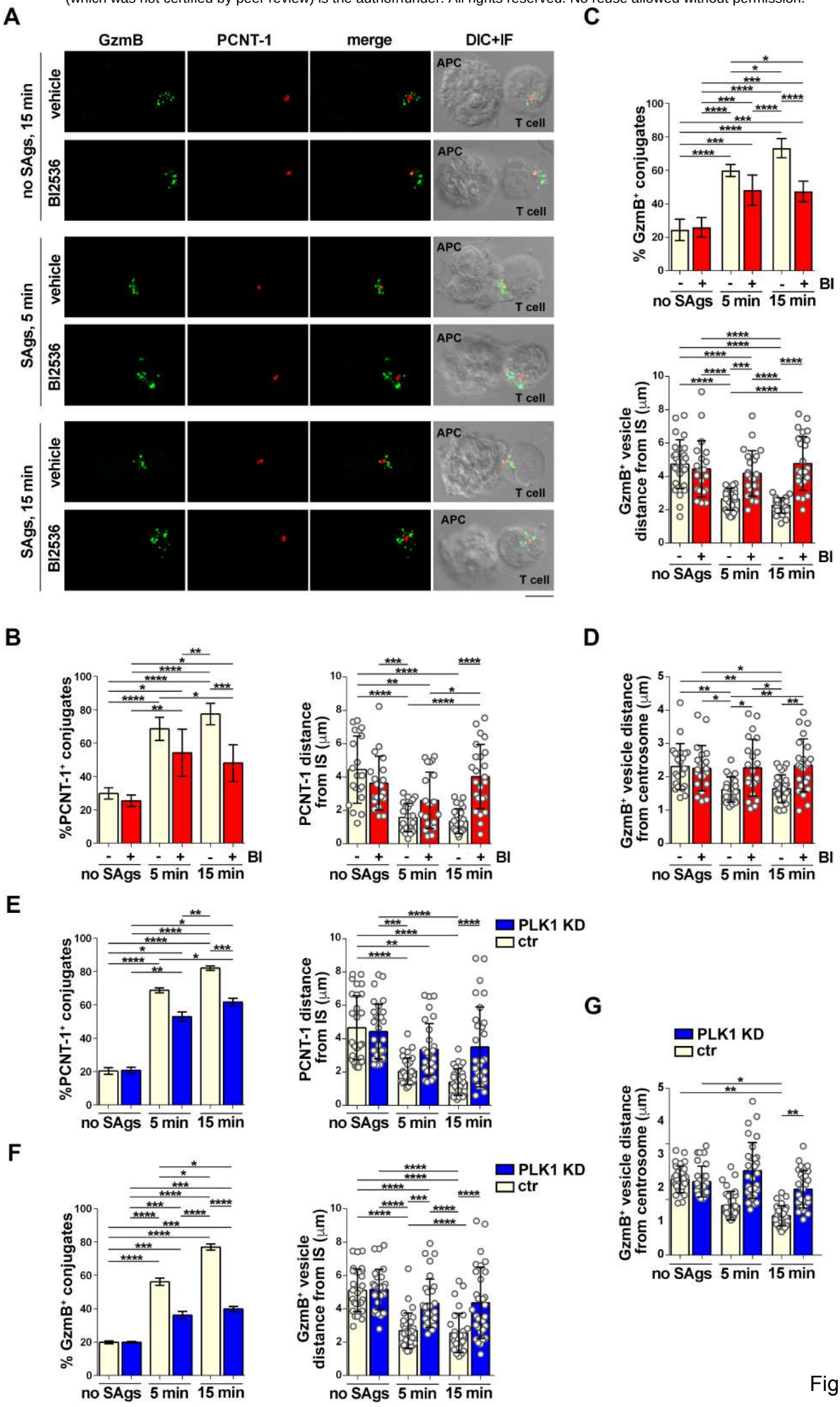

Figure 4

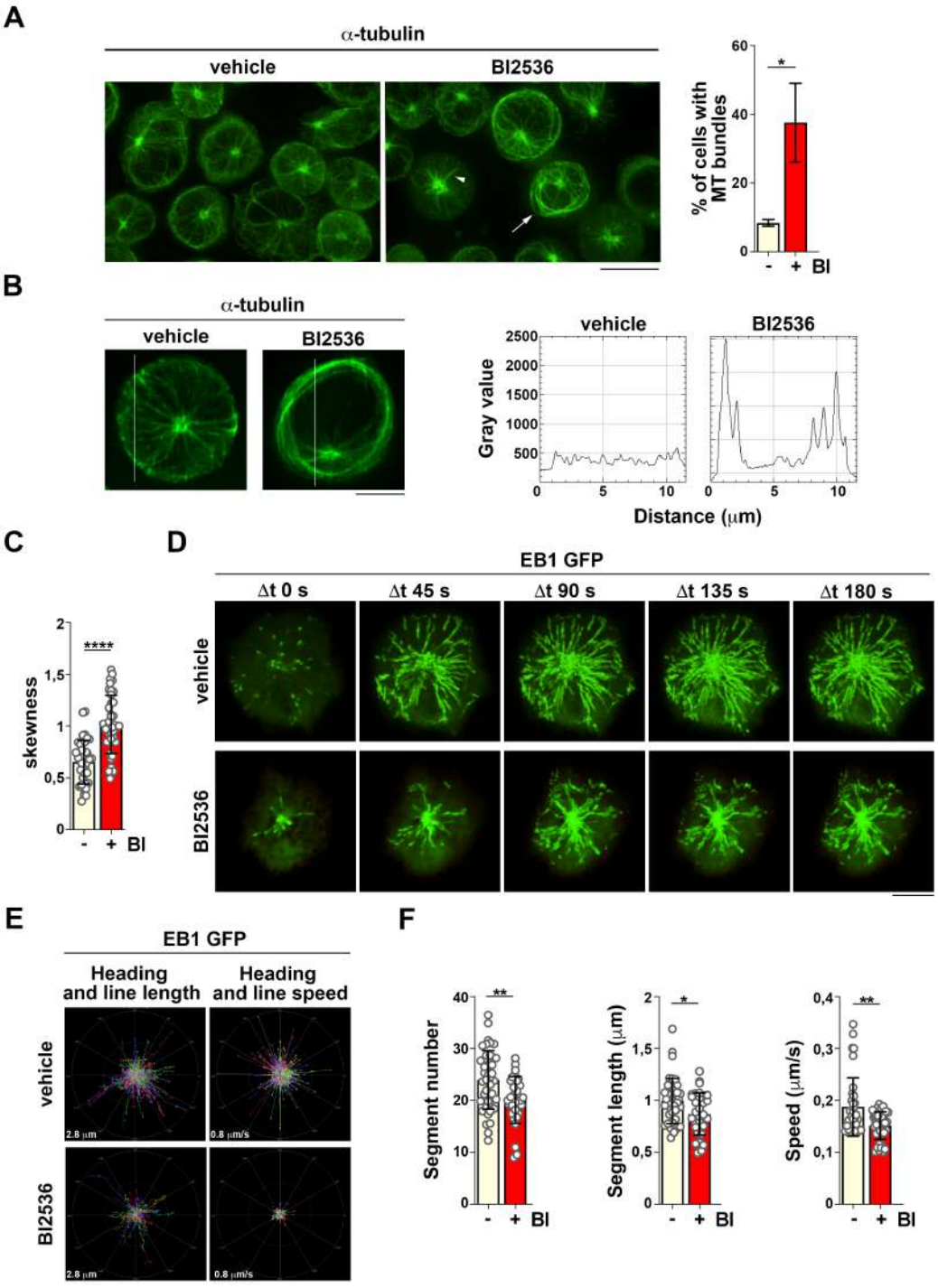

Figure 5

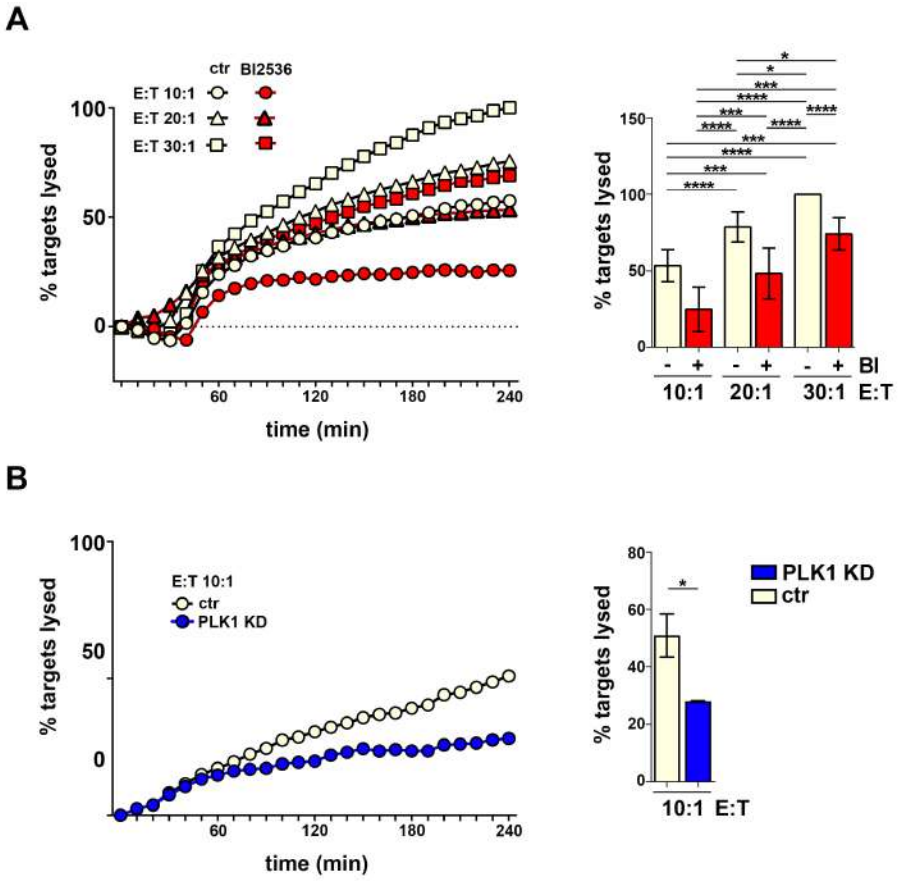

Figure 6